A. Romero-calvo, A.J. Garcia-salcedo, F. Garrone, I. Rivoalen, G. Cano-gomez, E. Castro-hernandez, M.A. Herrada Gutierrez, F. Maggi
StELIUM: a Student Experiment to Investigate the Sloshing of Magnetic Liquids in Microgravity
Acta Astronautica, Vol. 173, 2020, p. 344-355
doi:10.1016/j.actaastro.2020.04.013

Highlights

StELIUM: A student experiment to investigate the sloshing of magnetic liquids in microgravity

Á. Romero-Calvo,A. J. García-Salcedo,F. Garrone,I. Rivoalen,G. Cano-Gómez,E. Castro-Hernández,M. Á. Herrada Gutiérrez,F. Maggi

- The StELIUM project studies the lateral sloshing of ferrofluids in microgravity
- The experiment setup and drop tower campaign of StELIUM are described
- A dedicated surface reconstruction system is successfully designed and tested
- For the first time, a torque-generating setup is launched at ZARM's drop tower
- Sloshing control with magnetic liquids may apply to future space technology

StELIUM: A student experiment to investigate the sloshing of magnetic liquids in microgravity

Á. Romero-Calvo[a,b,*], A. J. García-Salcedo[b], F. Garrone[b], I. Rivoalen[b], G. Cano-Gómez[c], E. Castro-Hernández[d], M. Á. Herrada Gutiérrez[d] and F. Maggi[b]

[a]*Department of Aerospace Engineering Sciences, University of Colorado Boulder, CO, United States*
[b]*Space Propulsion Laboratory, Department of Aerospace Science and Technology, Politecnico di Milano, Via Giuseppe La Masa, 34, 20156, Milan, Italy*
[c]*Departamento de Física Aplicada III, Universidad de Sevilla, Avenida de los Descubrimientos s/n, 41092, Sevilla, Spain*
[d]*Departamento de Ingeniería Aeroespacial y Mecánica de Fluidos, Universidad de Sevilla, Avenida de los Descubrimientos s/n, 41092, Sevilla, Spain*

ARTICLE INFO

Keywords:
Magnetic liquid sloshing
Microgravity
Ferrofluids
Experiment design
ZARM's drop tower

ABSTRACT

Liquid sloshing represents a major challenge for the design and operation of space vehicles. In low-gravity environments, a highly non-linear movement can be produced due to the lack of stabilizing forces. This gives rise to significant disturbances that impact on the propulsion and attitude control systems of the spacecraft. The employment of magnetically susceptible fluids may open an interesting avenue to address this problem, but their dynamics in low gravity remain practically unexplored. The UNOOSA DropTES StELIUM project aims at filling this gap by studying the lateral sloshing of a ferrofluid solution subjected to an inhomogeneous magnetic field in microgravity. This paper describes the design process, challenges and preliminary results of the experiment, which was successfully launched at ZARM's drop tower in November 2019. The outcomes will be employed to validate the quasi-analytical models developed by the authors and set the path for the design of magnetic propellant positioning devices in space.

1. Introduction

The forced movement of liquids in partially filled tanks, commonly named sloshing, has been an active field of research for centuries. The first dynamic theory of tidal waves is attributed to Laplace as early as in 1775 (1), and the nonlinear wave problem was solved by Stokes in 1847 (2). By 1895, when the classical *Hydrodynamics* by Lamb was first published (3), there was already a solid heritage on the topic. The fundamental aspects of normal-gravity sloshing can be then considered to be well-established by the beginning of the Space Era, in 1957.

Propellant sloshing represents a major concern for space engineers (4). In extreme cases, like the Jupiter IRBM AM-1B (1957), the test vehicle F1 (1964) or the SpaceX Falcon 1 Demo Flight 2 (2007) (5), it may lead to a partial or total mission failure. Low-gravity sloshing is characterized by its highly stochastic and unpredictable dynamics, which result in a complicated propellant management system design and a complex impact on the attitude control system of the spacecraft. Moreover, propellant management devices increase the inert mass of the vehicle and present long-term reliability issues with cryogens (6; 7).

The sloshing of liquids in low-gravity is driven by surface tension and residual accelerations, that generate a curved equilibrium free surface (or meniscus) and a non-trivial interaction with the walls of the vessel (8). In the context of the Space Race, considerable efforts were devoted to the theoretical and experimental study of low-gravity sloshing (8; 9; 10; 11; 12; 13). These early works generally assume small, linear displacements around the equilibrium state. In most situations of interest for space applications, however, these assumptions do not hold, and complex Computational Fluid Dynamics (CFD) simulations become necessary (14; 15). In addition to their computational cost, numerical simulations rely on a good estimation of the initial conditions and accurate inertial measurements.

Different passive and active mitigation strategies have been traditionally employed to minimize low-gravity sloshing disturbances (6). An interesting alternative would be reproducing the restoring force of gravity by means of electromagnetic fields if the liquid can answer to such stimulus. That would transform a complex nonlinear sloshing problem into a linear, and hence easy to model, system. The use of *dielectrophoresis*, a phenomenon on which a force is exerted on dielectric materials in the presence of non-uniform electric fields, was explored by the US Air Force with suitable propellants in 1963 (16). The study unveiled a high risk of arcing inside the tanks and highlighted the need for large, heavy and noisy power sources. The inherent magnetic properties of paramagnetic and diamagnetic liquids may also be exploited in what is known as Magnetic Positive Positioning (MP^2) (17). Numerical simulations and microgravity experiments have been presented to validate this concept (18; 19).

The MP^2 concept must deal with the rapid decay of magnetic fields with distance, which limits its applicability to relatively small regions. This difficulty may be faced by employing highly susceptible magnetic fluids. Ferrofluids, defined as colloidal suspensions of magnetic nanoparticles in a carrier liquid, belong to this category and were indeed invented to enhance the susceptibility of rocket propellants in 1963 (20). However, contributions addressing their application to the control of liquid sloshing are scarce. Normal-gravity works have explored the natural frequency shifts due

*alvaro.romerocalvo@colorado.edu
ORCID(s): 0000-0003-3369-8460 (Á. Romero-Calvo)

Nomenclature

CCS	Capsule Control System
CFD	Computational Fluid Dynamics
DLR	German Aerospace Center
DropTES	Drop Tower Experiment Series
ELGRA	European Low-Gravity Research Association
ESA	European Space Agency
FEA	Finite Element Analysis
FFT	Fast Fourier Transform
GDS	General Detection Subsystem
HL	High Level
IAC	International Astronautical Congress
ISS	International Space Station
LED	Light-Emitting Diode
MAPO	Magnetically Actuated Propellant Orientation
MP^2	Magnetic Positive Positioning
NASA	National Aeronautics and Space Administration
PDU	Power Distribution Unit
PLA	Polylactic Acid
SD	Storage Device
SDS	Sloshing Detection Subsystem
SPLab	Space Propulsion Laboratory
StELIUM	Sloshing of magnEtic LIqUids in Microgravity
ToF	Time Of Flight
UNOOSA	United Nations Office for Outer Space Affairs
ZARM	Center of Applied Space Technology and Microgravity

to the magnetic interaction (21), two-layer sloshing (22), axisymmetric sloshing (23; 24), the swirling phenomenon (25) or the development of tuned magnetic liquid dampers (26; 27). The sloshing of ferrofluids in low-gravity was indirectly studied in 1972 with a focus on gravity compensation (28). In the mid 1990s, a series of parabolic flight experiments with ferrofluids were performed to validate the magnetic positioning of liquid oxygen in the framework of the NASA Magnetically Actuated Propellant Orientation (MAPO) experiment (17). Subsequent publications present refined numerical models for diamagnetic propellants (29; 30; 31). More recently, the ESA Drop Your Thesis! 2017 experimental campaign measured the axisymmetric sloshing of ferrofluids when subjected to an inhomogeneous magnetic field in microgravity (32; 33; 34). Quasi-analytical magnetic sloshing models (35) and feasibility analyses (36) have also been presented.

Based on the existing bibliography on the topic, the lateral sloshing of magnetic liquids in microgravity can be regarded as an almost unexplored phenomenon with potential applications in space. Those include passive MP^2, active MP^2 for center of mass positioning, and propellant sloshing damping, among others (36). Defining characteristics, such as the magnetic deformation of the meniscus or the shift of natural sloshing frequencies and damping ratios, have to be explored in relevant environments in order to improve our physics understanding and modeling capabilities.

With the goal of addressing the previous questions, in April 2019 the Sloshing of magnEtic LIqUids in Microgravity (StELIUM) experiment was selected by the United Nations Office for Outer Space Affairs (UNOOSA) Drop Tower Experiment Series (DropTES) programme to study the lateral sloshing of magnetic liquids in microgravity. This paper describes the project objectives (Sec. 2), selected microgravity facility (Sec. 3), experiment setup (Sec. 4), and preliminary results of the campaign at the drop tower of the Center of Applied Space Technology and Microgravity (ZARM) (Sec. 5). The main conclusions and future work are described in Sec. 6.

2. Experiment objectives

Experimental works on linear liquid sloshing have historically focused on the measurement of oscillation frequencies and modal shapes for different tank geometries and gravity levels (4; 6; 8). As previously stated, the sloshing of magnetic liquids in microgravity can be studied by assuming small oscillations through modal analysis (35). The design of StELIUM is consequently based on this methodology and has the following objectives:

1. Obtain high-quality free surface measurements of the lateral sloshing of a ferrofluid solution in microgravity when subjected to an inhomogeneous magnetic field.
2. Measure natural frequencies, damping ratios, modal shapes and meniscus profiles as a function of the external magnetic field.
3. Validate the inviscid quasi-analytical model developed by the authors (35) and share results with the scientific community.
4. Analyze the feasibility of magnetic sloshing damping techniques for space applications and other scenarios of interest in reduced-gravity environments.

The High-Level (HL) requirements of the experiment arise from the previous and are listed in Tab. 1.

3. Microgravity facility

3.1. On-ground microgravity platforms

The term *microgravity* refers to the residual relative acceleration between an observer and a target that fall simultaneously. In addition to on-orbit laboratories, such as the International Space Station (ISS), various on-ground facilities

Table 1
High-level requirements of StELIUM

ID	Requirement
HL-1	The lateral sloshing waves shall be excited in microgravity.
HL-2	The ferrofluid solution shall be subjected to a static, controllable and inhomogeneous magnetic field.
HL-3	The fundamental lateral sloshing frequency and damping ratio shall be measured.
HL-4	The second lateral sloshing frequency and damping ratio should be measured.
HL-5	The ferrofluid free surface shape shall be reconstructed.
HL-6	The equilibrium surface shape (or meniscus) shall be reconstructed.
HL-7	The experiment setup shall be monitored during the drop.
HL-8	The experiment setup shall withstand at least four catapult drops.
HL-9	The stability of the capsule shall be guaranteed.
HL-10	The experiment shall be integrated into the drop tower capsule

can replicate this condition. Each of them provides different gravity residuals g_{res} and flight durations $t_{\mu g}$, as summarized in Tab. 2.

Low gravity sloshing has been studied by making use of drop towers (37), parabolic flights (17), sounding rockets (38), on-orbit facilities (15) or simulated low-gravity (9; 28). The excessive gravity residual discourages the employment of parabolic flights, while on-orbit facilities are discarded due to their high cost and limited access. Sounding rockets offer several minutes of microgravity, but at a higher risk, as there is only one opportunity to perform the experiment. Thus, in order to obtain high-quality and repetitive measurements, ZARM's drop tower is selected to carry out the experiment.

3.2. ZARM's drop tower

With a 120 m high vacuum chamber, ZARM's drop tower is one of the largest on-ground microgravity facilities of its class in the world. The tower can operate with drop and catapult modes. In the first case, the capsule is released from the top giving 4.74 s of microgravity conditions and experiencing a deceleration of approximately 50 g_0 at the end of the flight. The catapult mode, available since 2007, launches the capsule vertically from the bottom of the tower extending the flight duration to 9.3 seconds. The capsule and its enclosed experiment experience an acceleration of up to 50 g_0 before the experiment begins, as shown in Fig. 1. Both modes are characterized by highest-quality conditions of weightlessness of approximately $10^{-6} g_0$.

Table 2
Characteristics of most relevant microgravity facilities

	Drop tower	Parabolic flight	Sounding rocket	ISS
$t_{\mu g}$	4.5-9.3 s	20-25 s	Minutes	Months
g_{res}	10^{-6}	10^{-2}	10^{-6}	10^{-6}
Frequency	2-4 drops/day	20-25 par/flight	1 exp/flight	-
Interaction	No	Yes	No	Yes
Cost	Low	Medium	Medium	High

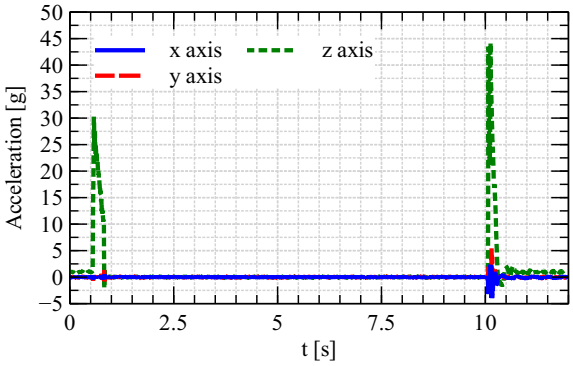

Figure 1: Acceleration profile of a catapult drop measured at ZARM's drop tower during the experiment campaign

The catapult capsule allows a maximum payload weight of 165 kg and a cylindrical payload volume with 600 mm diameter and 953 mm height. The system is monitored by the Capsule Control System (CCS), which is connected to the external control room through radio telemetry and telecommand to satisfy the HL-7 requirement. To ease integration, the experimental setup is mounted on a standardized platform. The capsule is carefully balanced before launch to avoid undesired perturbations. A constant environmental pressure level is kept during flight. Further specifications can be found at ZARM's Drop Tower User Manual (39).

Due to its extended low-gravity period, the catapult mode is selected for StELIUM. The design of the experiment must then consider an additional launch acceleration that induces an initial axisymmetric oscillation in the ferrofluid surface and imposes further restrictions to the structure.

4. Experiment setup

4.1. Historical review

Several drop tower experiments addressing low-gravity liquid sloshing have been carried out in the past. A non-extensive list may include the pioneering works by Satterlee and Reynolds (8) or the later contributions by Salzman and coworkers (37; 40). In spite of its age, the layout of Salzman's experiment setup is conceptually similar to StELIUM and hence of particular relevance for this project. His experiment used a DC engine to excite a test cylinder in microgravity (actuation system) illuminated by a diffuse backlight while a high-speed camera recorded the evolution of the surface (detection system). The experiment was mounted on a series of platforms that supported and protected each element (structure). In addition, this setup implemented a thruster to produce a range of gravity levels. Since StELIUM studies a prescribed range of magnetic field intensities, the functionality of the thrust system is here undertaken by a set

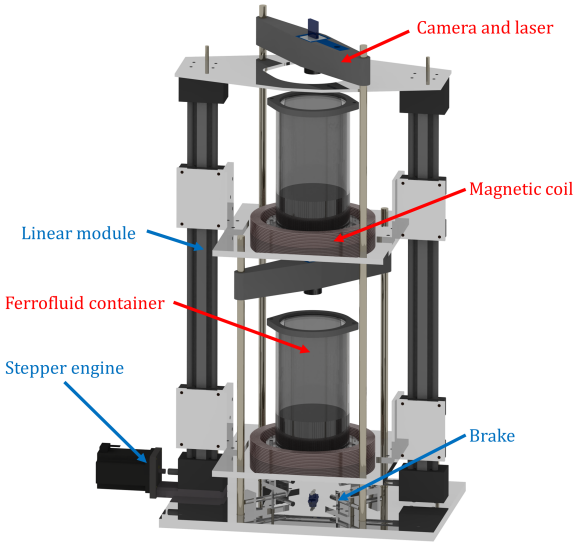

Figure 2: experiment setup of the ESA Drop Your Thesis! 2017 experiment *The Ferros*. Fixed and mobile parts are respectively labeled in blue and red. Adapted from (33).

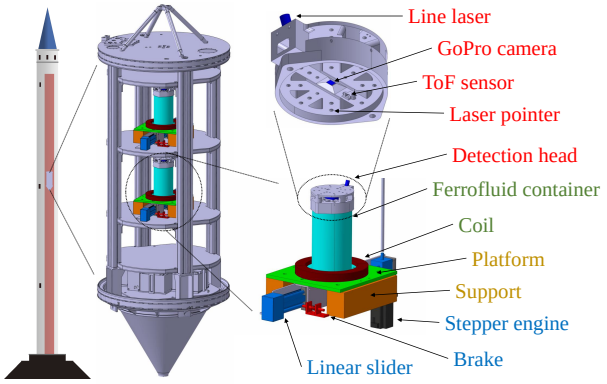

Figure 3: Experiment setup of StELIUM. The labels are grouped under the Sloshing Detection Subsystem (red), the Magnetic Subsystem (green), the structure (yellow), and the Actuation Subsystem (blue).

of coils (magnetic system).

A second setup of reference, this time designed for a parabolic flight, was used in the NASA MAPO experiment (17). The purpose of the project was to address the feasibility of magnetic propellant orientation devices and validate a custom CFD model in microgravity. The authors decided to employ a magnet whose magnetic field was mapped before running the experiment. Various oil-based ferrofluid solutions with different concentrations were then tested, but tended to coat the walls of the Plexiglas containers hampering visualization. In contrast, StELIUM employs a single ferrofluid solution under the action of a controllable magnetic field generated by a pair of coils. This choice reduces the overall cost of the experiment and avoids the irregularities in the magnetization field of most commercial magnets. To mitigate the aforementioned coating problems, water-based ferrofluids are employed together with an hydrophobic surface treatment on the walls of the containers (Aquapel).

The experiment setup of StELIUM is an evolution of the one employed at the ESA Drop Your Thesis! 2017 campaign (33), represented in Fig. 2. The setup made use of two coils in a quasi-Helmholtz configuration to generate the desired magnetic field. The actuation was carried out by a stepper engine controlled by an Arduino board. A pattern fringe reflectometry detection system was developed to measure the sloshing frequencies. However, the free surface shape could not be reconstructed due to the presence of strong light reflections (32). This experience has been considered for the design of StELIUM.

4.2. Overall description

From the systems engineering viewpoint, the experiment setup is subdivided into actuation, sloshing detection, magnetic, and structure subsystems. The actuation subsystem imposes a single lateral oscillation with prescribed amplitude (A) and frequency (ω) to a ferrofluid solution that partially fills a cylindrical container. The response of the liquid is measured by the Sloshing Detection Subsystem (SDS) to extract relevant kinematic parameters. During this process, the magnetic subsystem imposes a static, inhomogeneous magnetic field to the ferrofluid. Only the magnetic field intensity and actuation frequency vary between drops and, as described in Ref. (35), the sloshing frequencies vary accordingly. The structural configuration of the system is maintained throughout this process.

As shown in Fig. 3, the experiment setup is distributed between two capsule platforms that hold identical assemblies. Each of them is composed of a Plexiglas container surrounded by a magnetic coil which is fed by a constant current power source. The container has a diameter of 11 cm, a height of 20 cm and is filled up to 5 cm with a 1:5 volume solution of the Ferrotec EMG-700 water-based ferrofluid. Both assemblies are simultaneously actuated by a sliding mechanism that produces an oscillatory movement with a prescribed amplitude and frequency. The SDSs are located over each container and return a three dimensional liquid surface profile from which relevant parameters are extracted. Arduino based electronics powered by on-board batteries guarantee the autonomy of the system. The integrated setup is shown in Fig. 4.

The total mass of the experiment, including the additional platform, is approximately 60 Kg. The experiment setup fits into the available payload area with an overall volume of 930x530x295 mm^3, satisfying the requirement HL-10.

4.3. Drop tower plan

The experimental campaign at ZARM's drop tower is split into integration and experimentation weeks. The purpose of the first is to install and extensively test each subsystem to minimize the risk of failure during flight, given the limited number of drop opportunities. The second week is dedicated to performing the drops and running the experiment itself.

Figure 4: Drop tower capsule of StELIUM after integration at ZARM's drop tower

Four catapult drops were scheduled for StELIUM, with a rate of one per day. As explained in Sec. 4, the response of the liquid is analyzed as a function of the magnetic field intensity (or, equivalently, the coils current intensity I), which changes between drops. The first of them has the purpose of testing the performance of every subsystem and validating the amplitude of the actuation, which must induce an observable oscillation without reaching the non-linear regime. The following configurations, including the non-magnetic case, are shown in Tab. 3. During each flight, a single oscillation is induced 3 seconds after launch, when the surface reaches its equilibrium position. The frequency of such actuation is set between the first and second modes, so both are excited and measured by the SDSs.

4.4. Structure

The acceleration profile shown in Fig. 1 represents a technical challenge from the structural viewpoint. Finite Element Analyses (FEA) of critical structural parts become then mandatory to satisfy the requirement HL-8. Although the use of expendable components is extended in low-gravity research, this option was not considered appropriate for StELIUM.

The most critical structural parts are (i) the vessels containing the ferrofluid solution, and (ii) the sliding unions between the linear modules and the carriages that support the experiment setup. In the case of the vessels, a structural failure would release the ferrofluid content and potentially harm the electronics of the drop capsule. If the sliding unions were harmed, the oscillation produced by the actuation system would be much noisier.

A dynamic-implicit, two-dimensional, axisymmetric FEA is carried out in ABAQUS to analyze the stress and deformation of the Plexiglas vessel when subjected to a time-varying gravity load, as shown in Fig. 5. The mesh employs 2364 quadrilateral CAX4R elements with 1 mm edge length and 2683 nodes. A maximum Von Misses stress of 20 MPa is predicted during the drop sequence, but the tensile strength of Plexiglas is approximately 70 MPa. For safety reasons, lateral rods are added to hold the upper structure and distribute the loads.

A similar analysis is used to verify the resistance of the carriages with the simplified two-dimensional model depicted in Fig. 6. The combined weight of the ferrofluid vessel, magnetic coil, detection system, and platform is distributed among eight cylindrical unions that interface the assembly with the rails. Each union is composed of an inner plastic bearing located inside an aluminum holder. The properties of the plastic ring are assumed to be similar to the Igus Iglide J[1], whose maximum recommended surface pressure is 35 MPa. An encastre boundary condition is applied to the upper face of the plastic ring to simulate the presence of the rail. Quadrilateral (1542) and triangular (34) elements are employed in the mesh. The maximum compression stress suffered by the plastic ring is 8 MPa, while the aluminum

[1] https://www.igus.com/product/66. Consulted on: 30/01/2020

Table 3
StELIUM test matrix

Drop	ω (rad/s)	I(A)
1	6.5	20
2	3.3	10
3	3.3	0
4	5	15

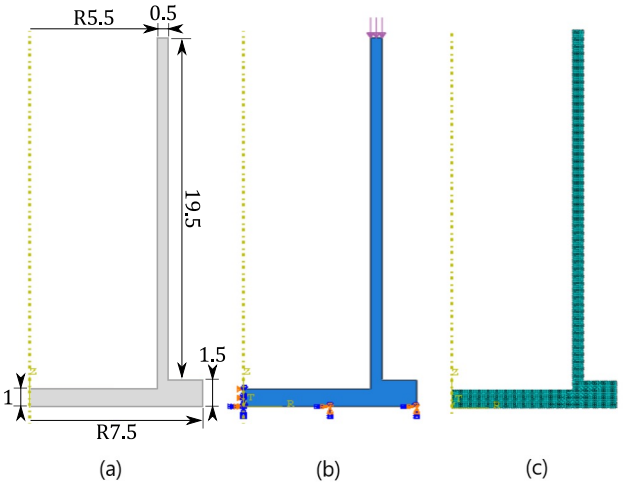

Figure 5: FEA model of the ferrofluid vessel. a) Geometry (units in cm), b) Loads and boundary conditions, c) Mesh.

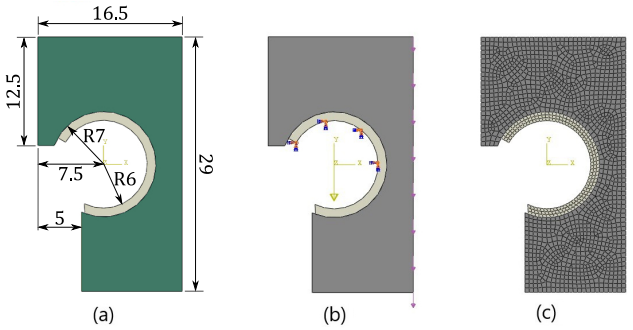

Figure 6: FEA model of the structural union. a) Geometry (units in mm), b) Loads and boundary conditions, c) Mesh.

box is subjected to a maximum stress of 1.1 MPa. Those values are far below the elastic limits of the materials. A sufficiently large safety margin is then present for both elements. However, important simplifying assumptions are taken in this analysis (e.g. 2D modeling of a 3D structure, that neglects 3D structural dynamics), and hence supports are added to the platforms to distribute the impact load.

During the drop campaign, the structure withstood four consecutive drops without apparent damages in either the Plexiglas vessels or the structural unions.

4.5. Magnetic subsystem

The magnetic setup produces a steady inhomogeneous magnetic field in the region where the ferrofluid is located, fulfilling the requirement HL-2. Such field generates a restoring force that keeps the liquid at the bottom of the container. This contribution can be decomposed as the sum of a magnetic body-force density

$$\mathbf{f}_V = \mu_0 M \nabla H, \tag{1}$$

with **H** being the magnetic field and **M** the magnetization field, and a surface-force density, also known as *magnetic normal traction*,

$$\mathbf{f}_S = \frac{\mu_0}{2} M_n^2 \mathbf{n}, \tag{2}$$

where M_n is the normal magnetization component at the interface of the ferrofluid (34; 41). It is important to note that the volume component appears only when an inhomogeneous field **H** is considered, since it depends on the gradient of H. Solutions with higher magnetic susceptibilities exhibit a stronger response.

As shown in Fig. 3, the magnetic field is generated by two circular coils located at the base of the vessels in a quasi-Helmholtz configuration. The coils have a diameter of 94.25 mm, a width of 25 mm and are built with 200 windings of a 1.8 mm copper wire. Their resistance increases during operation due to the rapid increase in temperature. In order to produce a static magnetic field, constant voltage power sources or batteries should then be discarded. A JT-DPM8600 constant current power source is employed instead, achieving an excellent performance.

Table 4
Properties of the Ferrotec EMG-700 solution and the 1:5 vol concentration solution at 25°C.

Property	Ferrotec EMG-700	1:5 Solution
Carrier liquid	Water	Water
Nature of surfactant	Anionic	Anionic
Nominal particle diameter (nm)	10	10
Saturation magnetization (kA/m)	25.86	4.16
Initial magnetic susceptibility χ	12.57	0.39
Viscosity (mPa.s)	<5	1.448
Density (kg/m^3)	1290	1058
Surface tension (mN/m)	N/A	45.7
Concentration of particles (%)	5.8	1.16

The magnetic liquid is provided by Ferrotec Corporation and consists on a 1:5 volume solution of the Ferrotec EMG-700[2] water-based ferrofluid. As explained in Sec. 4.1, low-viscosity water-based solutions are preferred over oil-based to avoid the severe coating effects reported in previous experiments (17). The properties of the original ferrofluid and the 1:5 volume solution are given in Tab. 4. The magnetization curve depicted in Fig. 7 was measured with a MicroSense EZ-9 Vibrating Sample Magnetometer at the Physics Department of Politecnico di Milano.

4.6. Actuation subsystem

The actuation subsystem induces an oscillatory liquid motion by imposing a sinusoidal displacement to the ferrofluid tank, hence addressing the requirement HL-1. The displacement is limited to 12 mm of amplitude for safety reasons, and the movement is configured to have an intermediate frequency between the first and second sloshing modes. This aims to excite the corresponding waves and unveil relevant kinematic parameters, like the actual modal frequencies.

The movement is transmitted as sketched in Fig. 8. Both containers are bolted to identical platforms that rest over two Igus ZLW-1040 linear modules. The sliding mechanisms are

[2] https://ferrofluid.ferrotec.com/products/ferrofluid-emg/water/emg-700-sp/. Consulted on: 30/01/2020

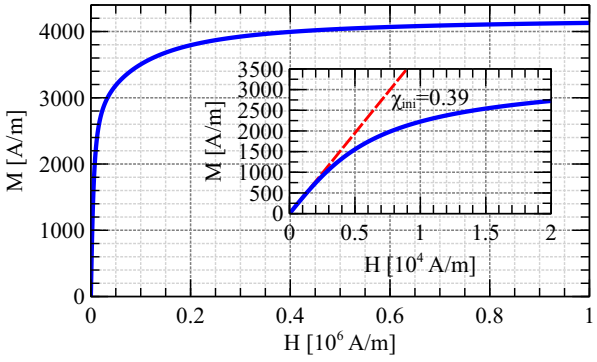

Figure 7: Experimental magnetization curve at 25°C of the 1:5 vol Ferrotec EMG-700 water-based ferrofluid solution

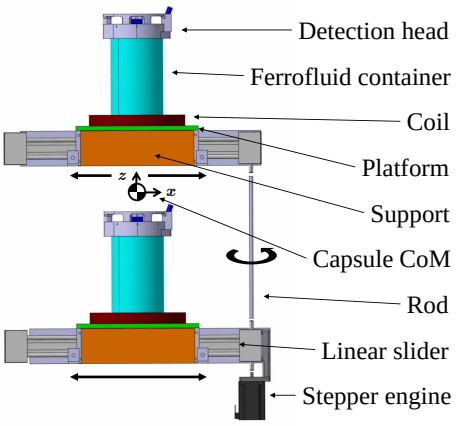

Figure 8: Operation of the Actuation Subsystem

actuated by highly resistant toothed belts connected to a vertical shaft. A Drylin NEMA-23 XL stepper engine located at the lower end of the shaft actuates the system. This configuration minimizes the number of moving parts and maintains the relative position between coils, hence avoiding undesired disturbances of the magnetic field. A single oscillation is imposed for each drop 3 seconds after launch, once the meniscus is stabilized after the initial acceleration peak.

The stepper engine is controlled by a Leadshine DM542 digital driver and an Arduino Nano board. The board implements a proportional control that computes the number of constant-velocity steps required to follow a sine wave. As a result, approximate wave profiles are obtained. This is shown in Fig. 9, where the slider displacement of the second launch is obtained from a VL6180X Time of Flight (ToF) sensor and compared with the expected sine wave. Since the 1-sigma bounds are 0.9510 mm in idle state and 1.1896 mm while the movement is produced, the measurements do not provide a reliable reconstruction of the movement, but confirm the sinusoidal profile.

To avoid unexpected displacements of the moving parts during launch and deceleration, a safety locking mechanism controlled by the CCS is installed. It is composed of a set

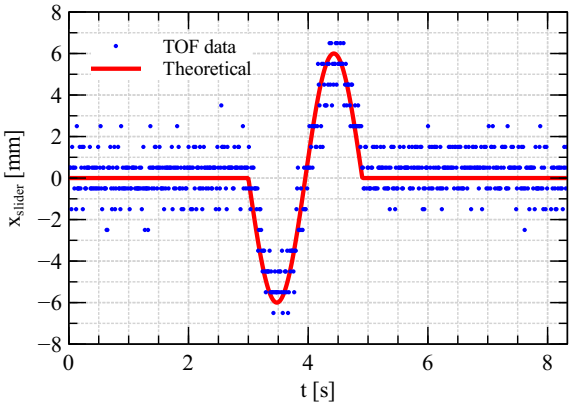

Figure 9: Lateral displacement of the sliders during the second launch

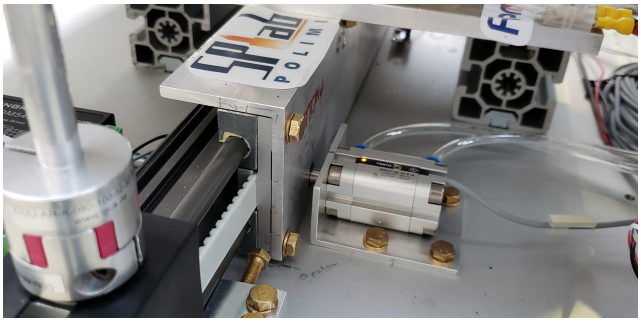

Figure 10: Pneumatic piston used to fix the moving assembly

of four pneumatic cylinders that block the platforms of the experiment at the beginning and end of the drop. One of them is shown in Fig. 10.

Liquid sloshing is modeled as the superposition of three spring-mass linear oscillators with natural frequencies $\omega_{n,1} = 4.6$ rad/s, $\omega_{n,2} = 10.2$ rad/s and $\omega_{n,3} = 10.3$ rad/s oriented in the direction of the actuation. The parameters of the system are obtained from a simplified low-gravity mechanical sloshing model with an effective gravity acceleration of 1 m/s^2 (6). This roughly approximates the effect of the magnetic force with a current intensity of 20 A. A damping co-

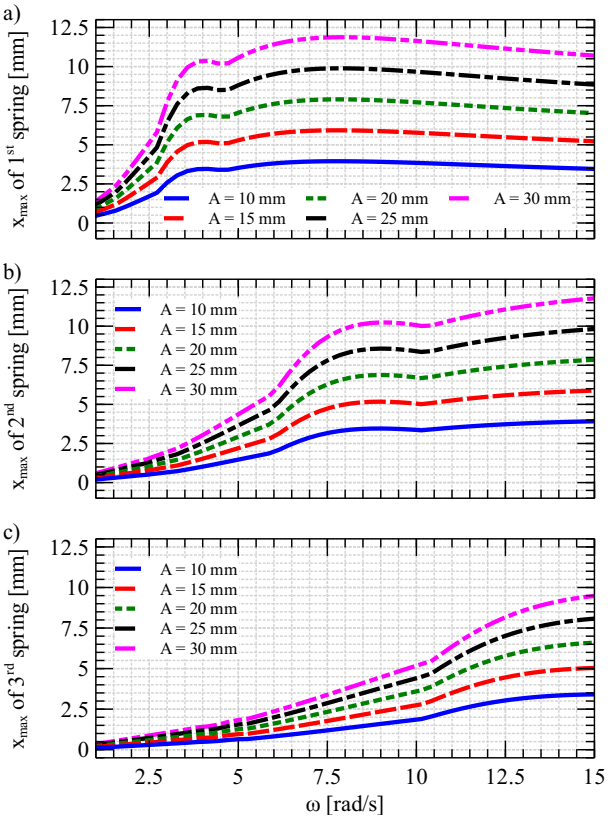

Figure 11: Maximum displacement of the a) fundamental spring-mass system, b) second spring-mass system, and c) third spring-mass system as a function of the frequency of the single-period quasi-sinusoidal excitation. The parameter of the plot represents the excitation amplitude.

efficient of 0.15 is assumed after analyzing the results of the precedent ESA Drop Your Thesis! 2017 - The Ferros experiment.

The maximum displacement of the i^{th} spring $x_{max,i}$ is depicted in Fig. 11 as a function of the excitation amplitude and frequency for a single-period quasi-sinusoidal excitation. It should be noted how, for excitation frequencies between $w_{n,1}$ and $w_{n,2}$, the first two modes are excited but the third remains relatively unperturbed.

4.7. Capsule stability

The lateral excitation displaces the center of mass and produces a disturbance torque that results in a temporary oscillation of the capsule. StELIUM is the very first experiment launched at ZARM's drop tower that produces this effect. A detailed analysis including worst-case scenarios becomes then mandatory to satisfy the requirement HL-9 and ensure a safe operation.

Two cases of analysis are here presented. In the regular scenario, both sliders move simultaneously in the same direction. Since the center of mass of the capsule is assumed to be placed just between them, only a small torque is generated by the oscillation of the liquid. In the worst-case scenario, one of the assemblies is blocked avoiding self-compensation, and the largest disturbance torque is produced. The most powerful actuation in Tab. 3, with a frequency approximately equal to 1 Hz, is assumed.

Figure 12 shows the regular scenario, a sine wave oscillation of 12 mm amplitude. The displacement of the sliders is represented in subfigure a). Subfigure b) depicts the displacement of the first three spring-mass sloshing analogies, the first and second being successfully activated. The horizontal position of the center of mass is illustrated in subfigure c). Finally, the torque induced by the movement is shown in subfigure d). Since both assemblies move simultaneously, this represents the worst case scenario for the displacement of the center of mass. However, it remains well within the 1 mm circle around the symmetry axis, as required by ZARM's drop tower user manual (39). The vertical position of center of mass of the capsule is assumed to be located just between the two moving assemblies, so the torque generated by the sliders is self-compensated. Since the center of mass of the moving fluid does not match that of the assembly, a residual component remains due to liquid sloshing. Moreover, if the vertical position of the center of mass is not located exactly between the platforms, a maximum tilting of $1.45{\cdot}10^{-5}$ deg/[mm of deviation] is obtained.

In an hypothetical critical scenario where the link between both sliders fails and only the bottom assembly is excited, a maximum tilting angle of less than 1° is ensured for excitation amplitudes lower than 25 mm and unfavorable vertical center of mass deviations below 150 mm.

The integrated capsule had a total mass of approximately 500 kg and a moving mass of less than 15 kg. Since an optimal vertical position of the center of mass could not be guaranteed, the displacement amplitude was limited to 12 mm for safety reasons. However, these values return a negligible tilting angle. This is verified with inertial data from the fourth drop, shown in Fig. 13. The upper plot shows the

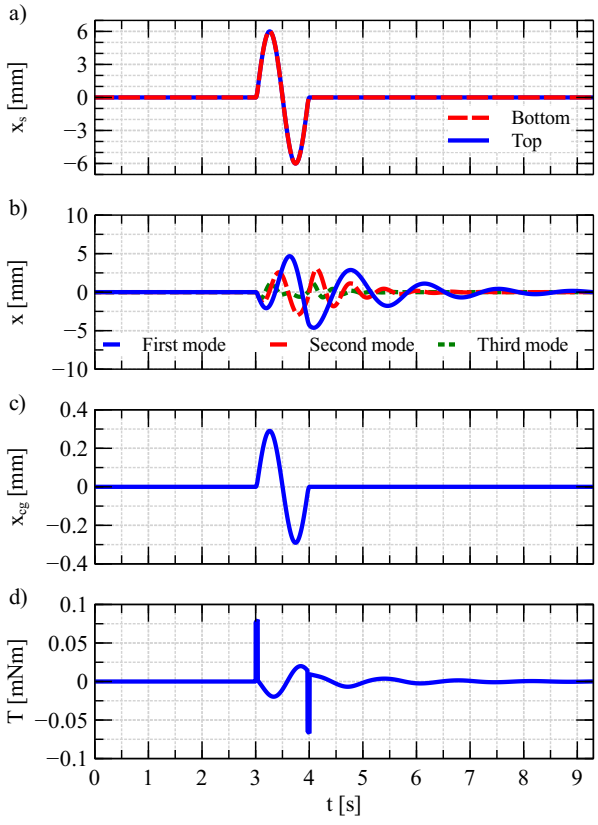

Figure 12: Regular scenario with optimum center of mass position. a) Slider displacement, b) springs displacement, c) capsule center of mass position, d) disturbance torque.

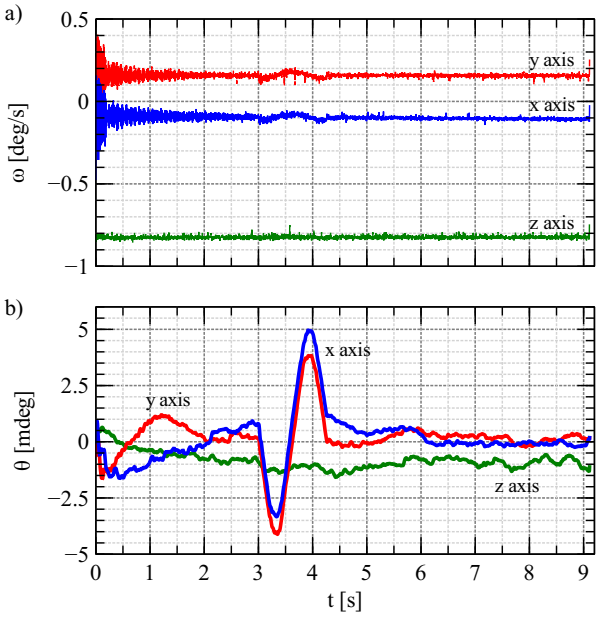

Figure 13: Inertial data of the fourth flight. a) Angular velocity, and b) mean-centered rotation imposed by the actuation.

evolution of the angular velocity, while the lower plot illustrates the mean-centered tilted angle induced by the excitation. The actuation effects can be observed between seconds 3 and 4.3, resulting in a maximum rotation of approximately 0.006 degrees. The requirement HL-9 is consequently satisfied, demonstrating for the first time the safe operation of a torque-generating experiment at ZARM's drop tower.

4.8. Detection subsystem

The detection subsystem includes all the components that measure the evolution of the liquid surface or relevant physical variables. It is composed of (i) the SDSs, (ii) two lateral cameras, (iii) two general visualization cameras, and (iv) the General Detection Subsystem (GDS).

The SDS, represented in Fig. 14, is the main component of the detection subsystem. Its goal is to reconstruct the liquid surface during flight, satisfying the requirements HL-3 to HL-5. A container cover with 20 laser diodes, a tilted line laser and a 4K resolution GoPro Hero 5 Session camera working at 30 fps conform the core of this device. The laser projections on the opaque ferrofluid surface are recorded by the camera, which correlates their apparent lateral displacement with the actual three-dimensional position of the surface. From the resulting kinematic evolution of each point, relevant parameters, such as modal shapes and frequencies, are computed. Furthermore, the liquid surface can be reconstructed with a set of suitable fitting functions to fulfill the requirement HL-4. The ideal accuracy of the system is below 0.4 mm for the laser pointers and 0.25 mm for the line laser.

The laser-based system is complemented by a VL53L0X ToF sensor, which offers a rough measurement of the fundamental sloshing frequency and enables a fast feedback between drops. An accelerometer is installed at the top of the container to complete the set of measurements required for validating CFD models. The signals from both sensors are continuously stored in the SD card with a sampling frequency of approximately 30 Hz. All the electronic elements are integrated in a 3D-printed PLA structure, which provides high structural resistance and geometrical adaptability. The reader is referred to Ref. (42) for a full description of the system, shown in Fig. 15.

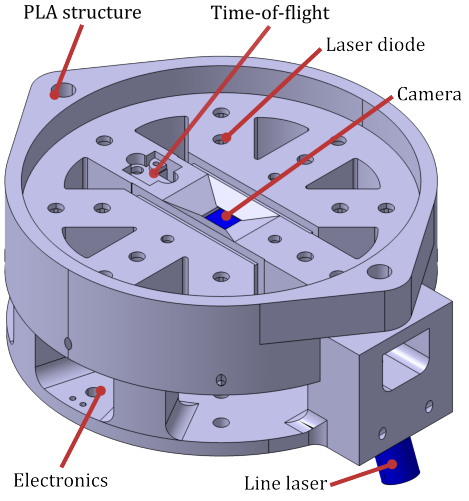

Figure 14: Bottom view of the Sloshing Detection Subsystem

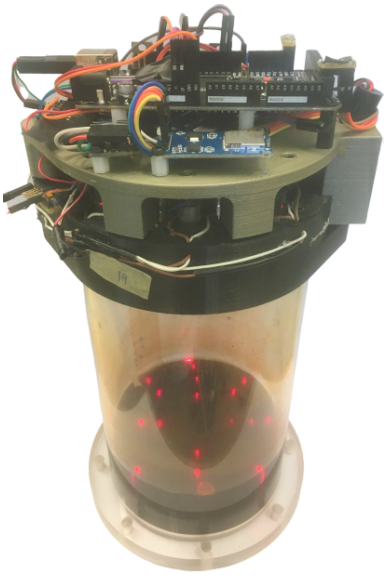

Figure 15: Image of the Sloshing Detection Subsystem integrated over the cylindrical ferrofluid container

The line laser, which is tilted a prescribed angle with respect to the axis of symmetry, projects a red line that crosses the center of the liquid surface. When the system enters microgravity conditions, the free surface and laser projection are deformed. The equilibrium surface can be then reconstructed by comparing both images, satisfying the requirement HL-6.

During the experimental campaign, the actuation mechanism produced a neat lateral oscillation of the surface. This allowed using the line laser alone to reconstruct the free liquid surface during the flight. Unlike the laser diodes, the high inclination of the line laser ensures a reflections-free observation of the liquid and improves the measurement resolution up to approximately 0.25 mm.

The SDSs are complemented with two Photron Fastcam MC2-10K lateral visualization cameras with SKR KMP-IR CINEGON 8 mm lenses working at 125 fps and 512×512 px^2 resolution. Their purpose is to serve as a backup system in case of total failure of the SDS. Additional general visualization cameras give a live feed of the experiment during the fight to satisfy the requirement HL-7. The GDS measures all the variables which are not directly related to the ferrofluid tanks (e.g. overall temperature, magnetic field intensity at selected locations, coils current intensity...). The measurements are continuously stored in a dedicated SD card.

4.9. Electronics

Arduino-based electronics are employed to control the different mechanisms of StELIUM and record relevant variables during the drop. Four different boards with separate

functionalities are powered by the Power Distribution Unit (PDU). The full electronic diagram of the experiment is shown in Fig. 19.

The Arduino boards are operated through of a LabView interface associated to the CCS. The launch sequence is programmed both in LabView and the Arduino boards. The former controls the cameras, trigger signals and braking mechanism, while the later receive the trigger, a single 5 V line, from the CCS. A first trigger signal is sent at the start of the drop sequence to synchronize the cameras with a LED blink and start the recording of scientific data at the SDSs and GDS. The detachment of the drop capsule from the catapult platform, which is produced in a window of 3 to 5 seconds from the start of the drop sequence, sends a second trigger to the boards. From this point, time delays are used to command the lateral excitation and stop data recording at the end of the drop. This system was proven to be robust and reliable.

The illumination inside the capsule is provided by a LED spotlight placed over the capsule platforms. This light was too bright to illuminate the ferrofluid surface without producing reflections at the surface, so a white panel was used instead to generate a diffuse homogeneous backlight, as shown in Fig. 4. Visualization from lateral cameras was significantly improved due to the higher contrast.

5. Preliminary results

Redundant measurements from the SDSs, GDS and lateral cameras were obtained for each drop. This focus on redundancy is key for any microgravity experiment, and was proven to be particularly useful for StELIUM. The high gravity accelerations induced partial subsystem failures in two of four drops, but the scientific results were never at risk. Although a detailed analysis of the data is still ongoing, the qualitative outcomes of the experiment are here presented.

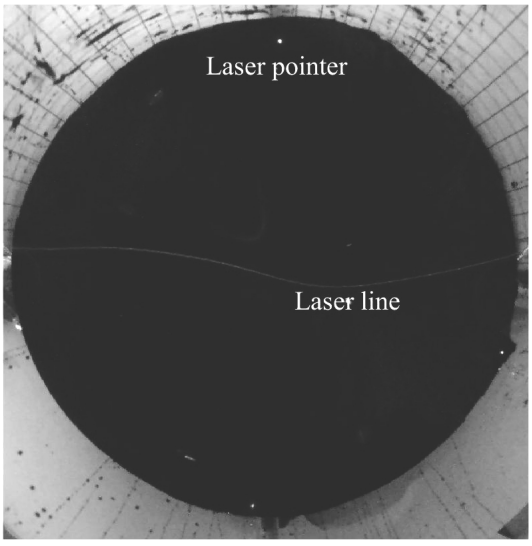

Figure 16: Top view of the ferrofluid surface from the main camera of the SDS

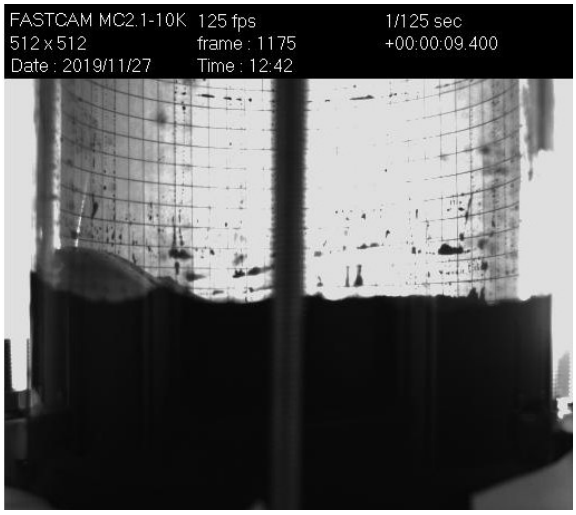

Figure 17: Lateral view of the ferrofluid surface from the high-speed camera

Figures 16 and 17 represent the top and lateral views of the upper container when the fundamental lateral sloshing wave of the second drop achieves its maximum amplitude. The deformation of the surface is deduced from the shape of the laser line. Two laser pointers, approximately located over the neutral line, are employed to detect undesired perpendicular disturbances. A preliminary analysis of their movement shows that such disturbances are indeed negligible and, consequently, that the laser line provides enough information to reconstruct the surface. Both images also reveal small ripples in the free surface contour, produced by the slight irregularities in the distribution of surface properties. Although undesired, their impact on the modal analysis is expected to be negligible.

Figure 18 depicts the Fast Fourier Transform (FFT) of the vertical displacement of each point of the laser line. As

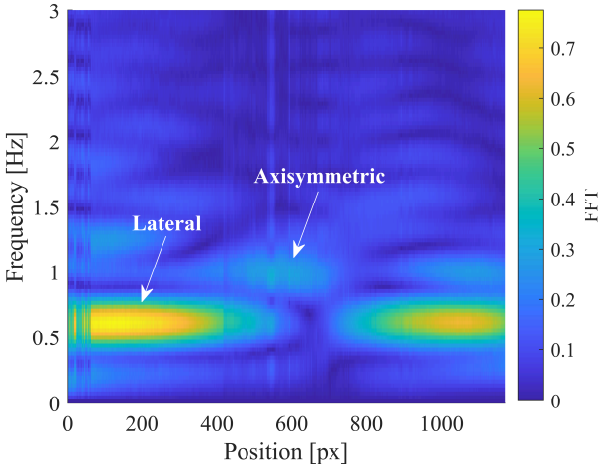

Figure 18: FFT of the vertical displacement of the laser line during the second drop. Lateral and axisymmetric modes are detected.

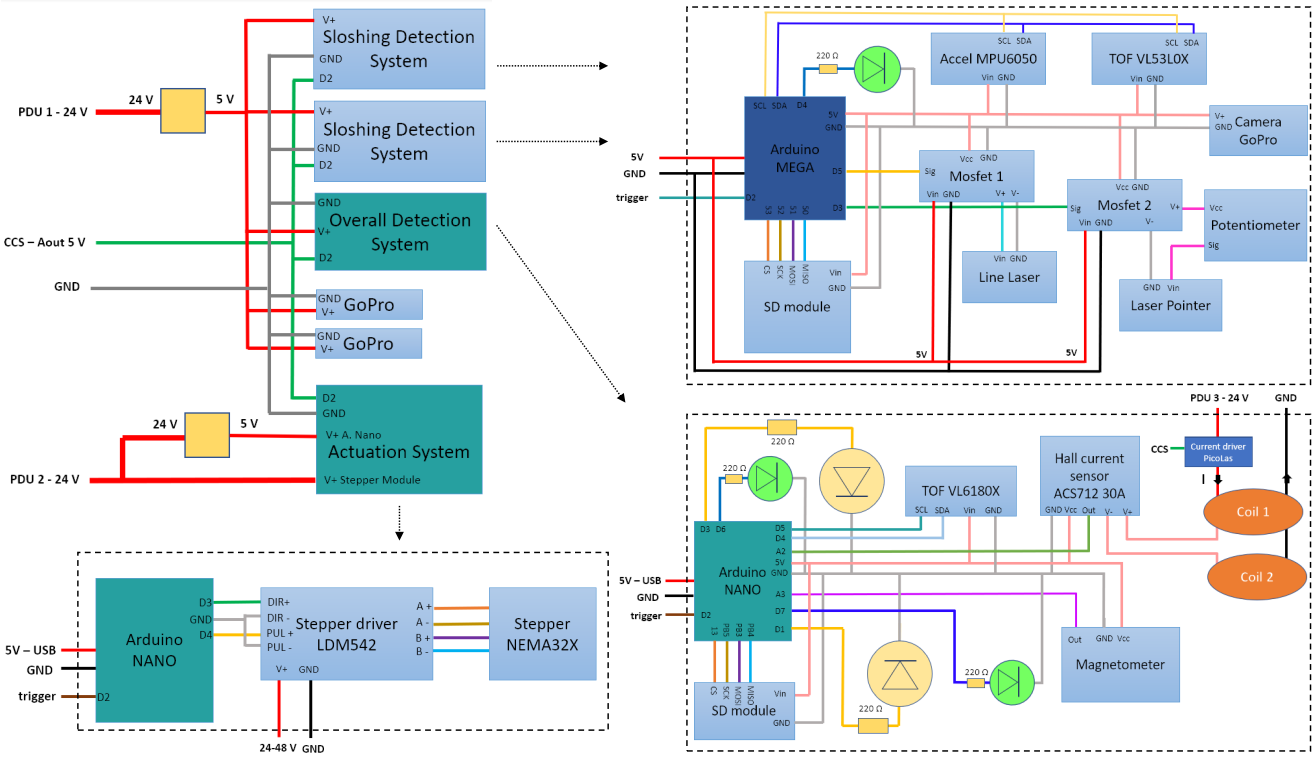

Figure 19: Electronic diagrams of StELIUM

expected, the center is only able to detect the axisymmetric sloshing wave, induced by the drop tower catapult and developed until the application of the lateral percussion at $t = 3$ s. The sides, on the contrary, reflect the fundamental and second lateral sloshing waves. It is important to note that the maximum amplitude is not produced at the contour, but at an intermediate radial position. Consequently, the edge follows an intermediate behavior between the *free* and *stuck* edge conditions described in Ref. (35).

6. Conclusions and future work

StELIUM was launched at ZARM's drop tower in November 2019 to study lateral sloshing of magnetic liquids in microgravity. This remains to be an almost unexplored phenomenon with potential applications in space. In this paper, the objectives, motivation, configuration, and preliminary outcomes of the project have been presented with a focus on its technical aspects.

The experiment setup has been described according to actuation, detection, magnetic and structure subsystems. Each of them contributes to the fulfillment of the high level requirements listed in Tab. 1 and, consequently, to the high-level objectives given in Sec. 2. Special attention has been payed to the development of the detection subsystem, that implements several redundant approaches to measure the kinematic evolution of the free liquid surface. The focus on redundancy an reliability has been key for the success of the drop tower campaign, that exposed the experiment setup to a highly demanding operational environment. StELIUM was also the very first experiment launched at ZARM's drop tower that imposed significant disturbance torques to the drop capsule. A dedicated stability analysis has been carried out to ensure that only minor oscillations are induced, as it was finally observed.

The meniscus profile, lateral and axisymmetric sloshing frequencies and operational variables (e.g. current intensity, acceleration, magnetic field intensity, etc) were recorded by different subsystems. The processed database will be employed to validate the magnetic sloshing model presented in Ref. (35). The outcomes of this experiment will be instrumental for increasing our understanding and modeling capabilities of this physical system, and may eventually pave the path for the development of new liquid management devices in space.

Competing Interests

The authors declare no competing interests.

Funding Sources

This work was supported by the United Nations Office for Outer Space Affairs (UNOOSA), the Center of Applied Space Technology and Microgravity (ZARM) and the German Space Agency (DLR) in the framework of the UNOOSA DropTES Programme 2019. Further financial and academic support was obtained from Ferrotec Corporation, Politec-

nico di Milano, the University of Seville, the European Space Agency (ESA) and the European Low Gravity Research Association (ELGRA).

Acknowledgements

The authors acknowledge the financial, technical and academic support offered by UNOOSA, DLR, ZARM, Ferrotec Corporation, Politecnico di Milano and the University of Seville. We also thank ESA and ELGRA for financing the presentation of this work at the 70th International Astronautical Congress (IAC) and the 26th ELGRA Biennial Symposium and General Assembly. This project is in debt with ZARM's drop tower engineers Jan Siemer and Fred Oetken, ZARM's point of contact Dr Thorben Könemann and UNOOSA's point of contact Ayami Kojima for their endless support. We finally thank the technicians Giovanni Colombo, Alberto Verga and the PhD student Riccardo Bisin from the Space Propulsion Laboratory (SPLab) of Politecnico di Milano for their academic and technical assistance, as well as the rest of members of this research group for contributing to the creation of an extraordinary professional and human environment.

References

[1] P. Laplace, Mémoires de l'Académie Royale des Sciences (88) (1775) 75–182.

[2] G. Stokes, On the theory of oscillatory waves, Transactions of the Cambridge Philosophical Society (8) (1847) 441–455.

[3] H. Lamb, Hydrodynamics, Cambridge University Press, 1895.

[4] W. C. Reynolds, H. M. Satterlee, The Dynamic Behavior of Liquids in Moving Containers, NASA SP-106, 1966.

[5] M. Eswaran, U. K. Saha, Sloshing of liquids in partially filled tanks - a review of experimental investigations, Ocean Systems Engineering 1 (2) (2011) 131–155.

[6] F. Dodge, The New Dynamic Behavior of Liquids in Moving Containers, Southwest Research Institute, 2000.

[7] J. G. Marchetta, Simulation of lox reorientation using magnetic positive positioning, Microgravity - Science and Technology 18 (1) (2006) 31.

[8] H. M. Satterlee, W. C. Reynolds, The Dynamics of Free Liquid Surface in Cylindrical Containers Under Strong Capillary and Weak Gravity Conditions, Report LG-2, 1964.

[9] F. T. Dodge, L. R. Garza, Experimental and Theoretical Studies of Liquid Sloshing at Simulated Low Gravity, Journal of Applied Mechanics 34 (3) (1967) 555–562.

[10] G. Yeh, Free and forced oscillations of a liquid in an axisymmetric tank at low-gravity environments, Journal of Applied Mechanics 34 (1) (1967) 23–28.

[11] P. Concus, G. Crane, H. Satterlee, Small amplitude lateral sloshing in spheroidal containers under low gravitational conditions, Vol. NASA-CR-72500, LMSC-A944673, 1969.

[12] F. T. Dodge, L. R. Garza, Simulated low-gravity sloshing in spherical, ellipsoidal, and cylindrical tanks, Journal of Spacecraft and Rockets 7 (2) (1970) 204–206.

[13] F. Dodge, Further Studies of Propellant Sloshing Under Low-Gravity Conditions, Vol. NASA-CR-119892, 1971.

[14] R. Luppes, J. Helder, A. Veldman, The numerical simulation of liquid sloshing in microgravity, in: H. Deconinck, E. Dick (Eds.), Computational Fluid Dynamics 2006, Springer Berlin Heidelberg, Berlin, Heidelberg, 2006, pp. 607–612.

[15] G. Lapilli, D. Kirk, H. Gutierrez, P. Schalhorn, B. Marsell, J. Roth, J. Moder, Results of microgravity fluid dynamics captured with the spheres-slosh experiment, in: Proceedings of the 66th International Astronautical Congress, Jerusalem, Israel, 2015.

[16] D. Chipchark, Development of expulsion and orientation systems for advanced liquid rocket propulsion systems, USAF Technical Report RTD-TDR-63-1048, Contract AF04 (611)-8200.

[17] J. Martin, J. Holt, Magnetically Actuated Propellant Orientation Experiment, Controlling fluid Motion With Magnetic Fields in a Low-Gravity Environment, 2000, NASA/TM-2000-210129, M-975, NAS 1.15:210129.

[18] N. Ramachandran, F. Leslie, P. Peters, R. Sisk, A novel method of gradient forming and fluid manipulation in reduced gravity environments, in: 36th AIAA Aerospace Sciences Meeting and Exhibit, 1998.

[19] J. Marchetta, A. Winter, Simulation of magnetic positive positioning for space based fluid management systems, Mathematical and Computer Modelling 51 (9) (2010) 1202 – 1212.

[20] S. Papell, Low viscosity magnetic fluid obtained by the colloidal suspension of magnetic particles, US Patent 3215572 (1963).

[21] S. Kaneko, T. Ishiyama, T. Sawada, Effect of an applied magnetic field on sloshing pressure in a magnetic fluid, Journal of Physics: Conference Series 412 (1) (2013) 012018.

[22] T. Ishiyama, S. Kaneko, S. Takemoto, T. Sawada, Relation between dynamic pressure and displacement of free surface in two-layer sloshing between a magnetic fluid and silicone oil, Materials Science Forum 792 (2014) 33–38.

[23] M. Ohaba, S. Sudo, Liquid surface behavior of a magnetic liquid in a container subjected to magnetic field and vertical vibration, Journal of Magnetism and Magnetic Material 149 (1995) 38–41.

[24] S. Sudo, H. Nishiyama, K. Katagiri, J. Tani, Interactions of magnetic field and the magnetic fluid surface, Journal of Intelligent Material Systems and Structures 10 (6) (1999) 498–504.

[25] T. Sawada, Y. Ohira, H. Houda, Sloshing motion of a magnetic fluid in a cylindrical container due to horizontal oscillation, Energy Conversion and Management 43 (3) (2002) 299–308.

[26] K. Ohno, M. Shimoda, T. Sawada, Optimal design of a tuned liquid damper using a magnetic fluid with one electromagnet, Journal of Physics: Condensed Matter 20 (20) (2008) 204146.

[27] K. Ohno, H. Suzuki, T. Sawada, Analysis of liquid sloshing of a tuned magnetic fluid damper for single and co-axial cylindrical containers, Journal of Magnetism and Magnetic Materials 323 (10) (2011) 1389 – 1393, proceedings of 12th International Conference on Magnetic Fluid, Sendai, Japan.

[28] F. T. Dodge, L. R. Garza, Free-surface vibrations of a magnetic liquid, Journal of Engineering for Industry 94 (1) (1972) 103–108.

[29] J. Marchetta, J. Hochstein, Fluid capture by a permanent ring magnet in reduced gravity, in: Proceedings of the 37th Aerospace Sciences Meeting and Exhibit, Reno, NV, USA, AIAA, 1999.

[30] J. Marchetta, J. Hochstein, Simulation and dimensionless modeling of magnetically induced reorientation, in: Proceedings of the 38th Aerospace Sciences Meeting and Exhibit, Renno, NV, USA, American Institute of Aeronautics and Astronautics, 2000.

[31] J. Marchetta, J. Hochstein, D. Sauter, B. Simmons, Modeling and prediction of magnetic storage and reorientation of lox in reduced gravity, in: 40th AIAA Aerospace Sciences Meeting & Exhibit, AIAA, 2002.

[32] A. Romero-Calvo, T. H. Hermans, G. C. Gómez, L. P. Benítez, M. H. Gutiérrez, E. Castro-Hernández, Ferrofluid dynamics in microgravity conditions, in: Proceedings of the 2nd Symposion on Space Educational Activities, Budapest, Hungary, 2018.

[33] A. Romero-Calvo, T. H. Hermans, L. P. Benítez, E. Castro-Hernández, Drop Your Thesis! 2017 Experiment Report - Ferrofluids Dynamics in Microgravity Conditions, European Space Agency - Erasmus Experiment Archive, 2018.

[34] A. Romero-Calvo, G. Cano-Gómez, T. H. Hermans, L. P. Benítez, M. Ángel Herrada Gutiérrez, E. Castro-Hernández, Total magnetic force on a ferrofluid droplet in microgravity, Experimental Thermal and Fluid Science (2020) 110124.

[35] A. Romero-Calvo, G. Cano Gómez, E. Castro-Hernández, F. Maggi, Free and Forced Oscillations of Magnetic Liquids Under Low-Gravity

Conditions, Journal of Applied Mechanics 87 (2) (2019) 021–010.
[36] A. Romero-Calvo, F. Maggi, H. Schaub, Prospects and challenges for magnetic propellant positioning in low-gravity, in: Proceedings of the AAS Guidance, Navigation and Control Conference, Breckenridge, Colorado, 2020.
[37] J. A. Salzman, W. J. Masica, Lateral Sloshing in Cylinders Under Low-Gravity Conditions, Vol. NASA TN D-5058, 1969.
[38] H. Gold, J. McArdle, D. Petrash, Slosh Dynamics Study in Near Zero Gravity, Vol. NASA TN D-3985, 1967.
[39] D. T. Operation, S. Company, ZARM Drop Tower User Manual, ZARM FABmbH, 2011.
[40] T. Coney, J. Salzman, Lateral sloshing in oblate spheroidal tanks under reduced- and normal-gravity conditions, Vol. NASA-TN D-6250, 1971.
[41] R. E. Rosensweig, Ferrohydrodynamics, Dover Publications, 1997.
[42] A. Romero-Calvo, A. García-Salcedo, F. Garrone, I. Rivoalen, G. C. Gomez, E. Castro-Hernández, F. Maggi, Free surface reconstruction of opaque liquids for experimental sloshing analyses in microgravity, in: Proceedings of the 70th International Astronautical Congress, Washington DC, USA, 2019.